APPLIED PHYSICS LETTERS **98**, 092503 (2011)

Competing effects of magnetocrystalline anisotropy and exchange bias in epitaxial Fe/IrMn bilayers

Wei Zhang,[1,a)] Mark E. Bowden,[2] and Kannan M. Krishnan[1,b)]
[1]*Department of Materials Science and Engineering, University of Washington, Seattle, Washington 98195, USA*
[2]*Environmental Molecular Science Laboratory, Pacific Northwest National Laboratory, Richland, Washington 99352, USA*

(Received 3 December 2010; accepted 8 February 2011; published online 1 March 2011)

We systematically investigated the possible magnetization reversal behavior in well-characterized, epitaxial, Fe/IrMn exchange-biased bilayers as a function of the antiferromagnetic (AF) layer thickness. Several kinds of multistep loops were observed for the samples measured at various field orientations. The angular dependence of the switching fields, observed using longitudinal and transverse magneto-optic Kerr effect, were shown to depend on the competition between the magnetocrystalline anisotropy and the exchange bias (EB). A modified "effective field" model was applied to quantitatively describe the evolution of the magnetic behavior and correctly predict the occurrence of different magnetic switching processes. The dependence of the effective anisotropy fields on the AF layer thickness directly reflects the competing effects of the pinned and rotatable AF spins at the EB interface. © *2011 American Institute of Physics*. [doi:10.1063/1.3561516]

The exchange bias (EB) (Ref. 1) effect, particularly in the form of a ferromagnetic (F)/antiferromagnetic (AF) bilayer, has been widely studied due to its applications in magnetic storage technologies.[2] One of the fundamental issues in EB is the spin behavior at the F/AF interface. Recent studies using synchrotron radiation[3] revealed the interfacial AF spins are either pinned, providing a hysteresis loop shift (H_{eb}), or rotatable, resulting in a coercivity (H_c) enhancement.[4–6] The values of H_{eb} and H_c intrinsically depend on the thicknesses of the F and AF layers.[7] Previous studies have shown that H_{eb} is roughly inversely proportional to the thickness of the F layer.[8] However, the dependence of H_{eb} on the AF layer thickness, t_{AF}, is complicated and largely depends on other parameters such as the material,[9] the setting field of EB,[10] and the temperature.[11]

Magnetic anisotropy is the fundamental physical parameter that determines the magnetization reversal processes.[12] Considering an unidirectional anisotropy, K_{eb}, and an induced uniaxial anisotropy, K_u, the value of H_{eb} and H_c for the polycrystalline EB systems can be numerically fitted by the Stoner–Wohlfarth model.[13] However, as compared to the extensive investigations on polycrystalline EB systems, only few works have focused on epitaxial bilayers,[14,15] which are, in fact, ideal systems for investigating EB due to the better control of the spin configuration at the interface.[4,16–19] In epitaxial EB systems, the intrinsic magnetocrystalline anisotropy results in multistep hysteresis loops and a complex angular dependent behavior.[14,15,20] An "effective field" model, taking into account the unidirectional anisotropy field, H_X, and the cubic F anisotropy field, H_A, was proposed to quantitatively interpret the angular dependent switching fields.[15] To date, however, the dependence of the magnetization reversal on t_{AF} in epitaxial EB systems has not been fully understood. In this work, we present a comprehensive study of the dependence of EB on t_{AF} for epitaxial Fe/IrMn bilayers. Different magnetic switching processes were found at various field orientations by vector magneto-optic Kerr effect (MOKE), which offers a comprehensive understanding of the magnetization reversal of the film by probing both the longitudinal and transverse magnetization components.[21,22] The evolutions of the angular dependent switching fields were interpreted by a modified effective field model. Peculiar dependence of both H_X and H_A on t_{AF} was observed and interpreted in terms of the competition between the pinned and rotatable interfacial AF spins.

A series of Fe/IrMn bilayers were grown on transparent MgO(001) substrates by ultrahigh vacuum ion beam sputtering with deposition rate as low as 1 Å/s, which is well suited for growing epitaxial magnetic thin films.[17,18] The substrates were preannealed at 500 °C for 1.5 h and held at 145 °C for deposition. A permanent magnet generating a field of ~300 Oe was positioned along the Fe[010] direction during growth. Samples with the structure of MgO/Fe(15 nm)/IrMn(t_{IrMn})/Ta(3nm, cap) were deposited with the IrMn layer thickness, $t_{IrMn}=0,2,3,4,4.5,5,5.5,6,8,10,14$ nm. The epitaxial relation of the samples was established using x-ray diffraction (XRD) with Cu $K\alpha$ radiation. In the θ-2θ scan [Fig. 1(a)], the (002) peaks of Fe and IrMn indicated a good out-of-plane (002) texture. Furthermore, the x-ray in-plane $\Phi-$scan [Fig. 1(b)] not only showed the fourfold symmetry but confirmed the epitaxial relationship of MgO(001)[100]∥Fe(001) [110]∥IrMn(001)[100].[23] Magnetic properties were probed *ex situ* at room temperature by vector MOKE and by illuminating the back side of the sample through the transparent substrates.

The anisotropy geometry and the magnetic switching routes used in this letter are summarized in Figs. 1(c) and 1(d). The EB gives rise to H_X and a collinear uniaxial anisotropy field, H_U, along the field cooling direction. Both of them are superimposed on H_A. Various switching routes between the Fe easy axes were observed using longitudinal (∥)

[a)] Electronic mail: zwei@uw.edu.
[b)] Author to whom correspondence should be addressed. Electronic mail: kannanmk@uw.edu.

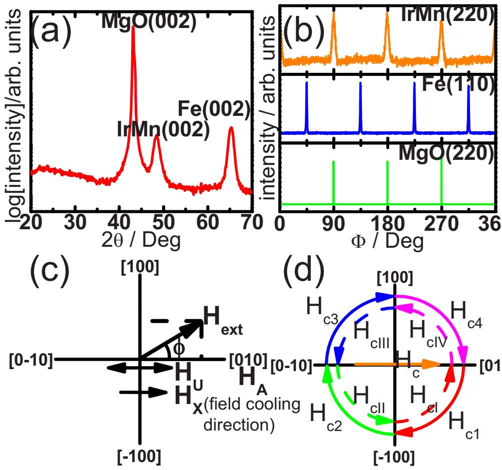

FIG. 1. (Color online) XRD measurements, (a) θ-2θ scan and (b) in-plane $\Phi-$scan, of the sample with $t_{IrMn}=14$ nm. (c) Geometry of the field cooling direction, magnetic anisotropies, and the external magnetic field. (d) Definition of the various switching fields between different Fe easy axes.

and transverse (⊥) MOKE loops obtained at different ϕ, which is the angle between the external applied field, H_{ext}, and the field cooling direction. Depending on the initial and final remanent directions involved in a magnetic transition, we refer [Fig. 1(d)] to the corresponding switching fields as H_{c1} to H_{c4} (clockwise), H_{cI} to H_{cIV} (counterclockwise), and H_c, respectively.

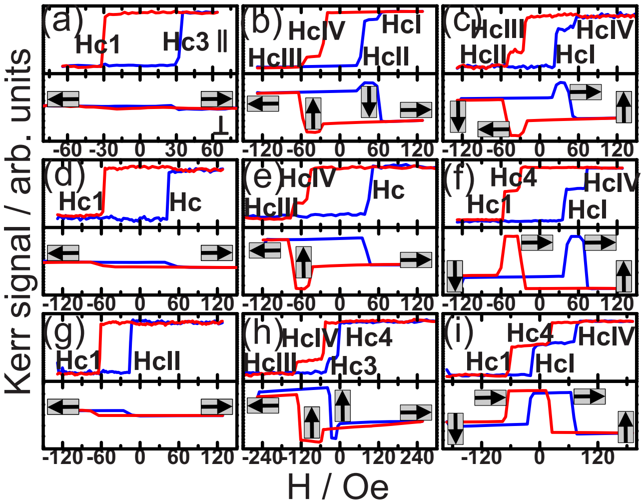

FIG. 2. (Color online) Typical longitudinal (∥) and transverse (⊥) MOKE loops measured at various field orientations for three samples with different t_{IrMn}. Results for 4 nm t_{IrMn} sample at (a) $\phi=0°$ (square loop), (b) $\phi=-30°$ (double-side two-step loop, opposite semicircles), and (c) $\phi=70°$ (double-side two-step loop, opposite semicircles). Results for 5 nm t_{IrMn} sample at (d) $\phi=0°$, (e) $\phi=-15°$ (asymmetrically shaped loop), and (f) $\phi=85°$ (double-side two-step loop, same semicircle). Results for 6 nm t_{IrMn} sample at (g) $\phi=0°$, (h) $\phi=-27.5°$ (double-side two-step loop, same semicircle), and (i) $\phi=82.5°$ (double-side two-step loop, same semicircle). The orientation of Fe spins in the switching processes is represented by the arrows enclosed in a square.

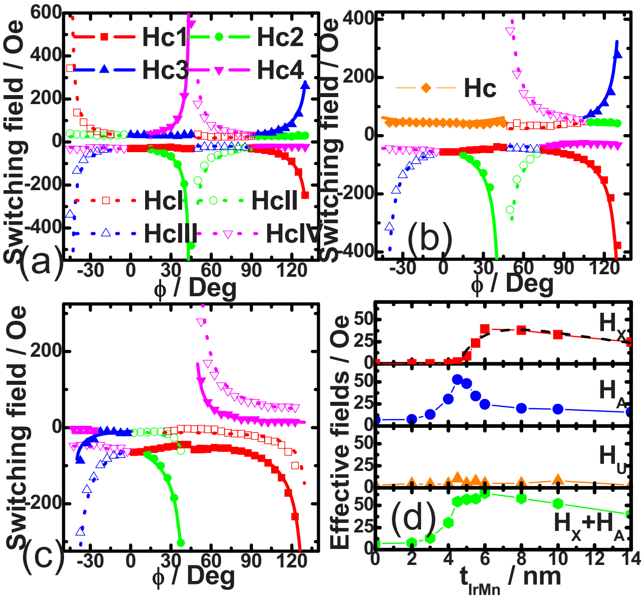

FIG. 3. (Color online) Typical field orientation dependence of the experimentally observed switching fields (symbols) and the corresponding theoretical fitting results (curves) for Fe/IrMn bilayers with (a) $t_{IrMn}=4$ nm, (b) $t_{IrMn}=5$ nm, and (c) $t_{IrMn}=6$ nm. The switching fields, represented by different symbols and curves, correspond to the magnetic transitions between different initial and final Fe easy axes orientations. (d) The effective anisotropy fields derived by the above fittings for Fe/IrMn bilayers with different t_{IrMn}. The dependence of H_X on t_{IrMn} was fitted (dash curve) by Eq. (9) in Ref. 9.

For samples with $t_{IrMn} \leq 4$ nm, the IrMn is too thin to establish a clear EB. Square loops [Fig. 2(a)] and double-sided two-step loops [Figs. 2(b) and 2(c)] were observed due to a weak H_U superimposed on the H_A.[24] The transverse MOKE signals revealed the magnetization reversal in the descending and ascending branches of the double-sided two-step loops are in opposite semicircles. The angular dependent behavior [Fig. 3(a)] looks symmetrical about H(y-axis)=0, ϕ(x-axis)=0° and 90° due to the weak EB and is similar to Fe/MgO(001) films.[25] For $t_{IrMn}=5$ nm sample, the loop measured at $\phi=0°$ starts to shift to the negative direction [Fig. 2(d)]. At close to $\phi=0°$, asymmetrically shaped loops were observed with two-step transitions for the descending branch but one-step for the ascending branch, Fig. 2(e). Perpendicular to the bias, for $45° < \phi < 135°$, two kinds of double-sided two-step loops can be observed. When ϕ is far away from 90°, the magnetization reversal for descending and ascending branches still occur at opposite semicircles; however, when ϕ is close to 90°, the magnetic switching routes for both branches are mediated via the same Fe easy axis determined by the bias [Fig. 2(f)]. The ϕ-dependent switching fields shows a clear asymmetry about $\phi=90°$ [Fig. 3(b)], showing the broken symmetry of anisotropy about $\phi=90°$ by the enhanced EB. As t_{IrMn} increases to 6 nm, the loop at $\phi=0°$ is completely shifted to the negative field regime [Fig. 2(g)]. Within $-45° < \phi < 45°$, a different type of double-sided two-step loop can be observed at ϕ away from 0° [Fig. 2(h)] with the magnetization reversal for both branches mediated via the same Fe easy axis. Within $45° < \phi < 135°$, all magnetization reversals are mediated via the same Fe easy axis superimposed by the bias, as shown in Fig. 2(i). In the $\phi-$dependent behavior, the symmetry about $\phi=90°$ is completely broken. For bilayers with $t_{IrMn} > 6$ nm, the magnetization reversal characteristics remains the same as the 6 nm t_{IrMn} sample.

We interpret the angular dependence of the switching fields by a modified effective field model. The switching fields can be derived by comparing the effective fields at the initial and final Fe easy axes involved in the magnetic transition.[15,20] The theoretical switching fields for 90°

magnetic transition can be obtained as follows: $H_{c1}=-(H_A+H_X+H_U)/(\cos\phi+\sin\phi)$, $H_{c2}=-(H_A+H_X-H_U)/(\cos\phi-\sin\phi)$, $H_{c3}=(H_A-H_X+H_U)/(\cos\phi+\sin\phi)$, $H_{c4}=(H_A-H_X-H_U)/(\cos\phi-\sin\phi)$, $H_{cI}=(H_A-H_X-H_U)/(\cos\phi+\sin\phi)$, $H_{cII}=(H_A-H_X+H_U)/(\cos\phi-\sin\phi)$, $H_{cIII}=-(H_A+H_X-H_U)/(\cos\phi+\sin\phi)$,$H_{cIV}=-(H_A+H_X+H_U)/(\cos\phi-\sin\phi)$. For 180° magnetic switching from the [0–10] to [010] axes, $H_c=(H_A-H_X+H_U)/\cos\phi$.

For samples with $t_{IrMn}\leq 4$ nm, the data can be nicely fitted by setting $H_X=0$ [Fig. 3(a)] due to the weak EB. It should be noted that, according to the reversal mechanism of two successive 90° magnetic transitions,[25] the switching fields for the square loop are fitted by H_{c1} and H_{c3}, but not H_c derived from 180° magnetization reversal. The one-step [Fig. 2(a)] and two-step [Fig. 2(b)] routes, for example in the case $-45°<\phi<0°$, correspond to $H_{cIII}>H_{cIV}$ ($H_{cI}<H_{cII}$) and $H_{cIII}<H_{cIV}$ ($H_{cI}>H_{cII}$) for decreasing (increasing) field, respectively. A nonzero H_X needs to be taken into account starting from the 5 nm t_{IrMn} sample [Fig. 3(b)]. For $-45°<\phi<45°$, a direct 180° magnetization reversal[20] becomes favorable instead of the two successive 90° magnetic transitions. For $70°<\phi<110°$, the magnetization reversal occurs along the same semicircle for descending (H_{c1},H_{c4}) and ascending (H_{cI},H_{cIV}) branches. Hysteresis loops revealed that $H_{c4}<0$, $H_{cI}>0$ at $\phi=90°$, therefore $H_A>H_X+H_U$, indicating that H_A is still the dominant effective field. As t_{IrMn} increased to 6 nm, the ϕ-dependent behavior was further modified [Fig. 3(c)]. Double-side, two-step loops were observed at $25°<|\phi|<45°$. The critical angle separating one-step to two-step reversal is different for descending and ascending branches. For example within $-45°<\phi<0°$, the critical angle is $-5°$ and $-25°$ for descending and ascending branch, respectively. Note that in this sample, $H_{c4}>0$, $H_{cI}<0$ at $\phi=90°$, indicating $H_X>H_A-H_U$, therefore H_X becomes the dominant effective field in the system.

Similar analyses on all the other samples were performed and the fitted effective fields are plotted in Fig. 3(d). For $t_{IrMn}\leq 4$ nm, $H_X=0$ and H_A displays a gradual enhancement with t_{IrMn}. For 4 nm$<t_{IrMn}<6$ nm, H_X rapidly increases, however, H_A decreases after reaching a peak at $t_{IrMn}=4.5$ nm. The sum of H_X and H_A remains at almost the same value for the range 4.5 nm$\leq t_{IrMn}\leq 6$ nm. The induced H_U is always very small, ~5 Oe, for all the samples. Our results on the t_{AF} dependence of H_X and H_A points directly to the competing effects of the pinned and rotatable AF spins at the interface.[4,26] For $t_{IrMn}\leq 4$ nm, the AF anisotropy is too weak to establish the bias. The AF spins at the interface only reverse with the F spins due to the strong exchange coupling, and contribute to the enhanced rotatable F anisotropy, H_A, rather than be pinned and create/enhance H_X. As t_{IrMn} further increases, some AF spins start to be pinned to provide H_X while H_A keeps increasing until $t_{IrMn}=4.5$ nm. Since the EB is an interfacial effect, the total number of pinned and rotatable spins reaches saturation at a certain t_{IrMn} value (4.5 nm in our case). Further increasing t_{IrMn} only results in more AF spins being pinned and less of them being rotatable. Thus an increase in H_X, but a decrease in H_A, can be observed for 4.5 nm$\leq t_{IrMn}\leq 6$ nm. The maximum exchange field, $H_X^m=40$ Oe is observed for $t_{IrMn}=6$ nm. Using the relation $\Delta E=H_X^m M_{Fe} t_{Fe}$ and the magnetization for bulk Fe, $M_{Fe}=1700$ emu/cm^3, and the Fe layer thickness, $t_{Fe}=15$ nm, the interface energy, ΔE, between Fe and IrMn is obtained as 0.102 erg/cm^2. The critical thickness for observing the EB, t_{AF}^{cr}, is ~4.5 nm from the data. According to the generalized Meiklejohn and Bean (MB) model,[9] the AF anisotropy, $K_{AF}=\Delta E/2\sqrt{2}t_{AF}^{cr}$,[9,27] is obtained as 0.8×10^5 erg/cm^3. For $t_{IrMn}>6$ nm, slight decrease in both H_A and H_X can be observed. The nonmonatomic dependence of H_X on t_{IrMn} can be described by the generalized MB model that takes into account the AF net magnetizations [Ref. 9].

This work was supported by DoE/BES under Grant No. ER45987. Part of the research was performed using EMSL, a user facility sponsored by DoE office of biological and environmental research located at PNNL. We thank Q. F. Zhan for helpful discussions.

[1] W. H. Meiklejohn and C. P. Bean, Phys. Rev. **102**, 1413 (1956).
[2] S. A. Wolf, D. D. Awschalom, R. A. Buhrman, J. M. Daughton, S. Von Molnar, M. L. Roukes, A. Y. Chtchelkanova, and D. M. Treger, Science **294**, 1488 (2001).
[3] G. Srajer, L. H. Lewis, S. D. Bader, A. J. Epstein, C. S. Fadley, E. E. Fullerton, A. Hoffmann, J. B. Kortright, K. M. Krishnan, S. A. Majetich, T. S. Rahman, C. A. Ross, M. B. Salamon, I. K. Schuller, T. C. Schulthess, and J. Z. Sun, J. Magn. Magn. Mater. **307**, 1 (2006).
[4] S. Brück, G. Schutz, E. Goering, X. Ji, and K. M. Krishnan, Phys. Rev. Lett. **101**, 126402 (2008).
[5] J. Wu, J. S. Park, W. Kim, E. Arenholz, M. Liberati, A. Scholl, Y. Z. Wu, C. Hwang, and Z. Q. Qiu, Phys. Rev. Lett. **104**, 217204 (2010).
[6] S. Brück, S. Macke, E. Goering, X. Ji, Q. Zhan, and K. M. Krishnan, Phys. Rev. B **81**, 134414 (2010).
[7] J. Nogués and I. K. Schuller, J. Magn. Magn. Mater. **192**, 203 (1999).
[8] R. Jungblut, R. Coehoorn, M. T. Johnson, J. aan de Stegge, and A. Reinders, J. Appl. Phys. **75**, 6659 (1994).
[9] C. Binek, A. Hochstrat, and W. Kleemann, J. Magn. Magn. Mater. **234**, 353 (2001).
[10] K. O'Grady, L. E. Fernandez-Outon, and G. Vallejo-Fernandez, J. Magn. Magn. Mater. **322**, 883 (2010).
[11] M. Ali, C. H. Marroas, M. Al-Jawad, B. J. Hickey, A. Misra, U. Nowak, and K. D. Usadel, Phys. Rev. B **68**, 214420 (2003).
[12] M. T. Johnson, P. J. H. Bloemen, F. J. A. den Broeder, and J. J. de Vries, Rep. Prog. Phys. **59**, 1409 (1996).
[13] J. Camarero, J. Sort, A. Hoffmann, J. M. Garcia-Martin, B. Dieny, R. Miranda, and J. Nogues, Phys. Rev. Lett. **95**, 057204 (2005).
[14] C. H. Lai, Y. H. Wang, C. R. Chang, J. S. Yang, and Y. D. Yao, Phys. Rev. B **64**, 094420 (2001).
[15] E. Arenholz and K. Liu, Appl. Phys. Lett. **87**, 132501 (2005).
[16] A. Mougin, S. Mangin, J. F. Bobo, and A. Loidl, Eur. Phys. J. B **45**, 155 (2005).
[17] N. Cheng, J. P. Ahn, and K. M. Krishnan, J. Appl. Phys. **89**, 6597 (2001).
[18] K. M. Krishnan, A. B. Pakhomov, Y. Bao, P. Blomqvist, Y. Chun, M. Gonzales, K. Griffin, X. Ji, and B. K. Roberts, J. Mater. Sci. **41**, 793 (2006).
[19] P. Blomqvist, K. M. Krishnan, and H. Ohldag, Phys. Rev. Lett. **94**, 107203 (2005).
[20] Q. F. Zhan, and K. M. Krishnan, J. Appl. Phys. **107**, 09D703 (2010).
[21] J. M. Florczak and E. D. Dahlberg, J. Appl. Phys. **67**, 7520 (1990).
[22] H. Ohldag, N. B. Weber, F. U. Hillebrecht, and E. Kisker, J. Appl. Phys. **91**, 2228 (2002).
[23] S. G. Wang, A. Kohn, C. Wang, A. K. Petford-Long, S. Lee, R. Fan, J. P. Goff, L. J. Singh, Z. H. Barber, and R. C. C. Ward, J. Phys. D: Appl. Phys. **42**, 225001 (2009).
[24] R. P. Cowburn, S. J. Gray, J. Ferre, J. A. C. Bland, and J. Miltat, J. Appl. Phys. **78**, 7210 (1995).
[25] Q. F. Zhan, S. Vandezande, K. Temst, and C. V. Haesendonck, New J. Phys. **11**, 063003 (2009).
[26] F. Radu, A. Westphalen, K. Theis-Brohl, and H. Zabel, J. Phys.: Condens. Matter **18**, L29 (2006).
[27] A. L. Kobrinskii, A. M. Goldman, M. Varela, and S. J. Pennycook, Phys. Rev. B **79**, 094405 (2009).